



HAL
open science

Estimation of Parasitic Capacitance of Common Mode Noise in Vehicular Applications: An Unscented Kalman Filter-Based Approach

Sepehr Karimi, Ebrahim Farjah, Teymoor Ghanbari, Farshid Naseri, J-L. Schanen

► **To cite this version:**

Sepehr Karimi, Ebrahim Farjah, Teymoor Ghanbari, Farshid Naseri, J-L. Schanen. Estimation of Parasitic Capacitance of Common Mode Noise in Vehicular Applications: An Unscented Kalman Filter-Based Approach. IEEE Transactions on Industrial Electronics, 2021, 68 (8), pp.7526–7534. 10.1109/TIE.2020.3007088 . hal-03651563

HAL Id: hal-03651563

<https://hal.science/hal-03651563>

Submitted on 17 Jun 2022

HAL is a multi-disciplinary open access archive for the deposit and dissemination of scientific research documents, whether they are published or not. The documents may come from teaching and research institutions in France or abroad, or from public or private research centers.

L'archive ouverte pluridisciplinaire **HAL**, est destinée au dépôt et à la diffusion de documents scientifiques de niveau recherche, publiés ou non, émanant des établissements d'enseignement et de recherche français ou étrangers, des laboratoires publics ou privés.

Estimation of Parasitic Capacitance of Common Mode Noise in Vehicular Applications: An Unscented Kalman Filter-Based Approach

Sepehr Karimi, Ebrahim Farjah, *Member, IEEE*, Teymoor Ghanbari, *Member, IEEE*, Farshid Naseri, *Student Member, IEEE*, and Jean-Luc Schanen, *Senior Member, IEEE*

Abstract—Parasitic capacitance has a considerable impact on conductive electromagnetic interference (EMI), especially on the common mode (CM) noise. In vehicular applications such as More Electric Aircraft and Electrical Vehicles, the value of CM stray capacitance can vary during the drive cycle, due to some change in environmental and operating conditions, resulting in fluctuations in EMI level. Designing EMI filters according to potentially overestimated CM capacitance results in additional weight, volume, and cost which should be avoided. In this paper, for the first time, the parasitic capacitance relevant to CM noise is estimated in real-time using Unscented Kalman Filter (UKF). The UKF is employed due to its ability in dealing with nonlinearity and stochastic nature of the EMI as well as the measurement noises. The proposed method is tested on a typical DC-DC buck converter in different operating conditions. The effectiveness of the proposed method is tested using some Hardware-in-the-Loop (HIL) experiments using dSPACE1104 development platform.

Index Terms—Electromagnetic Interference (EMI), State Estimation, Unscented Kalman Filter (UKF)

I. INTRODUCTION

NOWADAYS, the use of Switch Mode Power Supplies (SMPSs) in vehicular applications such as More Electric Aircrafts (MEAs) and Electric Vehicles (EVs) is increasing due to their high efficiency, small size, and low cost. However, in such applications, the immunity of the equipment to EMI is more critical due to continual variations of the Electromagnetic Interference (EMI) sources during a typical drive cycle of the vehicular system. Therefore, electromagnetic compatibility (EMC) of the components in such systems should be preserved in different operating conditions. Several research works have so far been fulfilled regarding the EMI problems of vehicular applications [1]-[3]. An important aspect of the EMI is the conducted emission, which can be categorized into the

differential mode (DM) and common mode (CM) noises. The study of the CM noise characteristics and CM noise cancellation techniques have been active research areas in recent years, which are briefly reviewed in the following:

In [4], conducted EMI modeling of the DC-DC buck converter with SiC JFET-based semiconductor switch has been fulfilled in the time-domain using the Saber™ simulation environment. It is confirmed that the proposed model is suitable for EMI prediction in ultra-fast switching SiC-based converters. A detailed CM noise model that considers all the parasitic capacitances in low-power AC-DC converters has been developed in [5]. Based on this model, it was confirmed that two critical CM noise sources of the converter are dv/dt on the input capacitor and bridge rectifier diodes. To achieve a more detailed EMI analysis, it is necessary to use EMI models considering all the existing parasitic capacitances [6]-[9]. In [10], an EMI model has been proposed for the cable and return current path including the parasitic capacitances of a motor drive system and cables in a hybrid EV. In [11], an effective EMI model has been developed to analyze the impacts of the AC motor feeding cables parameters on the parasitic capacitances and CM current. In [12], the impacts of different cable arrangements and lengths on the generated transient overvoltages and CM currents have been characterized in PWM motor drives. The EMI modeling of the inverter, cables, and the induction motor in variable speed drives using a chain of quadripolar matrices has been fulfilled in [13]. Using this model, the currents generated by the parasitic elements can be predicted in different stages of the matrix chain. To reduce the undesirable CM noise effects, a CM voltage cancellation (CMVC) method based on magnetic coupling has been proposed in [14]. In [15], the effects of parasitic capacitances on the CM noise level in a boost power factor correction converter and LLC resonant converter have been analyzed.

The foregoing review reveals that parasitic capacitances have a considerable impact on the level of the CM noise [16]-[19]. There are different parasitic capacitances in the power electronics circuits such as the parasitic capacitances between the gate-source, gate-drain, and drain-source of MOSFETs. These parasitic capacitances, however, mostly influence the switching behavior of the semiconductor switches [20]-[21]. On the other hand, the CM noise is mostly affected by the parasitic capacitances between the drain of the MOSFET to the

Place for Footnote

ground, the parasitic capacitance of the cable, and the parasitic capacitance between the drain of the MOSFET to the heatsink [22]. The values of these capacitances depend on some design characteristics and distance between the drain and reference ground. Indeed, connections/disconnections of the loads, vibrations of cables, etc. result in variation of these capacitances and CM emission levels. Two basic approaches for offline measurement of the parasitic capacitance have been proposed, which are based on the time domain reflectometry (TDR) [23] and impedance spectroscopy [24]. In [25], the estimation of the parasitic capacitance using the Least Squares (LS) linear regression technique has been addressed, where the LS method is applied to a set of basic measurements. In addition to the measurement-based approaches, some simulation-based methods have also been proposed, which include methods based on printed circuit board modeling and using Maxwell Q3D software [26].

All of the foregoing approaches are offline and they have some significant challenges to be developed as online techniques in real-time. Furthermore, offline measurement of stray capacitances is not suitable for a full study of CM capacitance variation in real operating conditions. Thus, EMI filters may not be optimally designed, if CM capacitance change. In [29], the Extended Kalman Filter (EKF) has been used for the online estimation of the parasitic capacitances. However, this method is not applicable for estimation of the parasitic capacitance in the EMI context but rather is proposed for Electrochemical sensors applications. Online calculation or measurement of the parasitic capacitance may find a high degree of importance in special applications such as More Electric Aircrafts (MEAs) and EVs. In such applications, the environmental and operating conditions such as temperature, vibrations, humidity, etc. can change during a drive/flight cycle. According to simulation and experimental studies in past works, variations of these parameters can change some key parameters that will indirectly affect the value of the parasitic capacitance. For example, in [27]-[28], it has been shown that the accumulation of dust, dirt, etc. can change the dielectric constant, which increases the parasitic capacitance leading to enhanced EMI level. The real-time estimation of the parasitic capacitance is a nice solution to study CM capacitance in real operating conditions (monitoring and recording during a whole mission profile, thereby obtaining the range of variations). Another application could be the use of this estimation combined with an active filter to compensate for CM current.

Estimation of the effective parasitic capacitance in CM noise is the main contribution of this work, which, to the best of the authors' knowledge, is being addressed for the first time. The real-time estimation of the parasitic capacitance provides several advantages, a few of them are discussed as follows:

- 1- The proposed technique can be used to obtain a long time recording of the parasitic capacitance, which is worthwhile to achieve an optimal EMI filter design with lower size, weight, and volume.
- 2- When the CM parasitic capacitance increases, the resonance frequency between the parasitic capacitance and the system inductances moves toward the system carrier frequency, which can lead to a substantial increase of the CM current when the resonance

frequency is excited. By continuous monitoring of the CM parasitic capacitance, such conditions can be effectively avoided.

To achieve the foregoing objective, first, the equivalent circuit model of the CM noise for a typical DC-DC buck converter is derived. Using this model together with the Unscented Kalman Filter (UKF) algorithm, the parasitic capacitance is estimated in an online manner. The UKF is adopted due to its excellent performance characteristics in random and noisy conditions. The rest of this paper is organized as follows:

In Section II, the CM noise model of the DC-DC buck converter is presented. Some discussions regarding the influencing factors on the parasitic capacitance are also included in this section. In Section III, the operating principles of the proposed UKF-based approach are discussed in detail. Several simulations and some real-time Hardware-in-the-Loop (HIL) experiments are fulfilled and the results are provided and discussed in Section IV. Some discussions regarding the computational time of the proposed algorithm are provided in Section V. The practical challenges of the proposed approach are discussed in Section VI. Finally, the main conclusions and future work are discussed in Section VII.

II. CONDUCTED EMI OF DC-DC BUCK CONVERTER

For real-time estimation of the CM parasitic capacitance, in the first step, the equivalent circuit model of the CM noise for the target power electronics converter should be derived. Although the proposed approach can be used with different converter topologies, for simplicity of analysis and to facilitate the understanding of the proposed approach, a typical DC-DC buck converter is selected for the study. In the following subsections, the CM noise equivalent circuit of the under-study converter is derived and some factors that affect the value of the parasitic capacitance are discussed.

A. CM noise equivalent circuit of DC-DC buck converter

The schematic of the DC-DC buck converter and the associated parasitic capacitances are shown in Fig. 1. In Fig. 1, C_1 is the parasitic capacitance between node A and the ground, C_2 is the parasitic capacitance between node B and the ground, C_P is the parasitic capacitance between the drain and the ground, and C_{cable} is the parasitic capacitance between the cable and the ground. Referring to Fig. 1, one can write [30]:

$$C_T = C_1 + C_2 \quad (1)$$

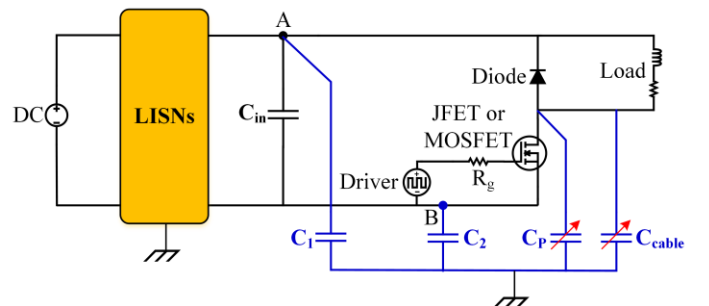


Fig. 1. Schematic of the DC-DC buck converter with parasitic capacitances

$$C_{CM} = C_P + C_{cable} \quad (2)$$

To analyze the conducted EMI of the DC-DC buck converter, the detailed form of Fig. 1 is depicted in Fig. 2, where the schematic of the line impedance stabilization networks (LISNs) and the paths for conducted EMI noises are also shown. Based on the current path of the CM noise in Fig. 2, the CM equivalent circuit model of Fig. 3(a) is obtained [4], [31]. Since the main target of this paper is estimation of the parasitic capacitance relevant to the CM noise, we focus only on the CM noise model. Referring to Fig. 3(a), one can write:

$$V_{Total} = V_{DS} \cdot \frac{C_{CM}}{C_{Total}} \quad (3)$$

$$C_{Total} = C_{CM} + C_T \quad (4)$$

Based on (3) and (4), the Thevenin equivalent circuit of Fig. 3(a) can be obtained as shown in Fig. 3(b). In Fig. 3(b), the CM current can be written as follows:

$$i_{CM} = \frac{V_{Total}}{\frac{1}{2}R_{LISN} + Z_{C_{Total}}} \quad (5)$$

where $Z_{C_{Total}}$ is impedance of C_{Total} , determined as follows:

$$Z_{C_{Total}} = \frac{1}{j\omega C_{Total}} \quad (6)$$

Considering $R_{LISN} \ll Z_{C_{Total}}$, (5) is approximated as follows:

$$i_{CM} \approx \frac{V_{Total}}{Z_{C_{Total}}} = V_{DS} \cdot j\omega C_{CM} \quad (7)$$

Therefore, the CM voltage can be obtained as follows:

$$V_{CM} \approx \frac{1}{2}R_{LISN} V_{DS} \cdot j\omega C_{CM} \quad (8)$$

According to (8), the parasitic capacitance C_{CM} has the dominant impact on the CM voltage, and the effects of the other parasitic capacitances can be neglected. Therefore, it can be seen that the CM noise equivalent circuit model of Fig. 2 converges to the simplified circuit of Fig. 3(c). In this work,

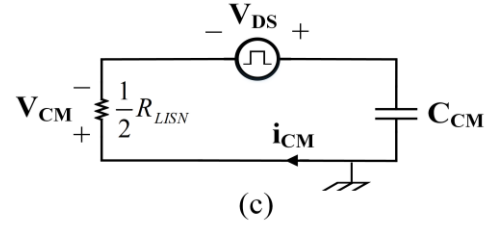
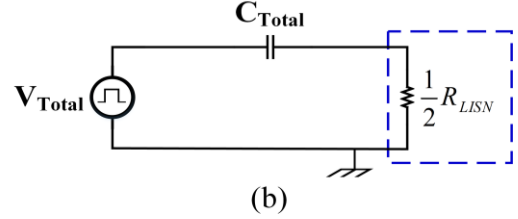
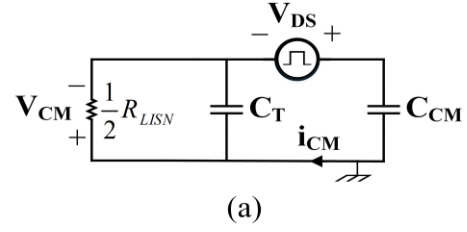


Fig. 3. (a) Equivalent circuit for CM conducted EMI noises (b) Thevenin equivalent circuit for CM noise (c) Simplified equivalent circuit of CM

this equivalent circuit model is used for real-time estimation of C_{CM} , which has the main contribution in CM noise. Since V_{DS} and V_{CM} are measurable in the equivalent circuit, C_{CM} can be estimated by a suitable estimator.

B. Influencing factors on the parasitic capacitance

During a road cycle, various factors such as vibration, humidity, and temperature, influence the value of the parasitic capacitance. In [32], these influencing factors are analytically formulated for calculation of the per-length parasitic capacitance in printed circuit boards (PCBs) as follows:

$$C = \frac{2.85\epsilon_{eff}}{\text{Ln} \left(1 + \frac{1}{2} \frac{8h}{w_{eff}} \left[\frac{8h}{w_{eff}} + \sqrt{\frac{64h^2}{w_{eff}^2} + \pi^2} \right] \right)} \quad (F / \text{length}) \quad (9)$$

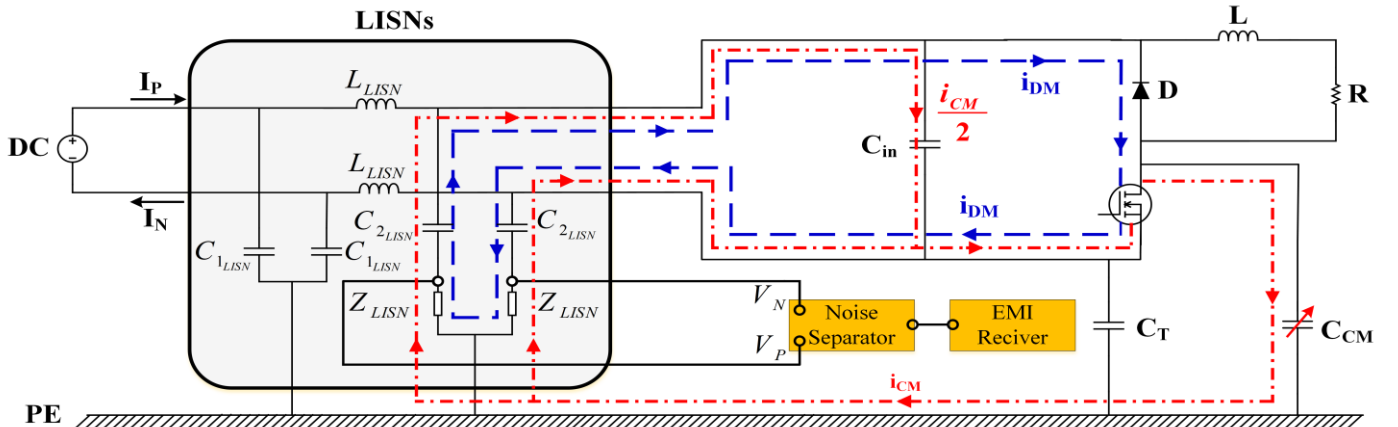


Fig. 2. Detailed form of Fig. 1 including the schematic of the LISNs and current paths for DM and CM noises in the studied DC-DC buck converter

$$w_{eff} = w + \frac{t}{\pi} \operatorname{Ln} \left(\frac{4e}{\sqrt{t^2 + \frac{1}{\pi^2 (w/t + 1.10)^2}}} \right) \quad (10)$$

$$\epsilon_{eff} = \frac{\epsilon_r + 1}{2} + \frac{\epsilon_r - 1}{2} \left(1 + \frac{10h}{w} \right)^{-1/2} \quad (11)$$

where w , l , and t denote the width, length, and thickness of the traces in PCBs, respectively. Also, h is the distance between the traces to ground in PCBs. Moreover, ϵ_r , ϵ_{eff} and w_{eff} are dielectric constant, effective dielectric constant, and effective width, respectively. For a typical signal trace with $t=0.0254$ mm (0.001 inches), $w=5$ mm (0.19685 inches) and different dielectric constants, the variation of the parasitic capacitance as a function of h and ϵ is shown in Fig. 4(a). It can be observed that slight changes in h , which for instance, can occur due to vibrations, lead to significant variation of the parasitic capacitance. This impact is more considerable when h is very low and the vibrations are relatively intense. According to [34], the capacitance of cable at height h above the ground, with length l and radius r , can also be calculated as follows:

$$C = \frac{2\pi l \epsilon_r \epsilon_0}{\cosh^{-1} \left(\frac{h}{r} \right)} \quad (F) \quad (12)$$

EVs and/or MEAs may experience different operating conditions in a typical road/flight cycle, which can potentially increase the dielectric constant. For instance, the sediment of some containments like carbon dioxide and salt can change the capacitance. In Fig. 4(b), the parasitic capacitance of a typical wire with $r=3.33$ mm ($A=35$ mm², an example of high-voltage EVs cables) and $l=5$ m when the substrates are affected by pollutants including $\epsilon_{CO2}=1.6$, $\epsilon_{Sand(Dry)}=5$, and $\epsilon_{Clay}=1.8-2.8$ is shown. Fig. 4(b) clearly shows that the parasitic capacitance can potentially change with variation of h or dielectric constant.

The aforementioned analysis shows that the value of the parasitic capacitances can change during a typical mission-profile of the vehicular system. In the next section, a novel approach for online estimation of this varying CM parasitic capacitance is proposed.

III. PROPOSED METHOD FOR ESTIMATION OF THE PARASITIC CAPACITANCE

In the first step, the equivalent circuit model of Fig. 3(c) should be written in the state-space form. Writing KVL in the equivalent circuit model of Fig. 3(c) yields:

$$-V_{DS} + V_{C_{CM}} + \frac{1}{2} R_{LISN} (2i_{C_{CM}}) = 0 \Rightarrow -V_{DS} + V_{C_{CM}} + R_{LISN} C_{CM} \frac{dV_{C_{CM}}}{dt} = 0 \quad (13)$$

Equation (13) can be rewritten as follows:

$$\frac{dV_{C_{CM}}}{dt} = \frac{-1}{R_{LISN} C_{CM}} V_{C_{CM}} + \frac{1}{R_{LISN} C_{CM}} V_{DS} \quad (14)$$

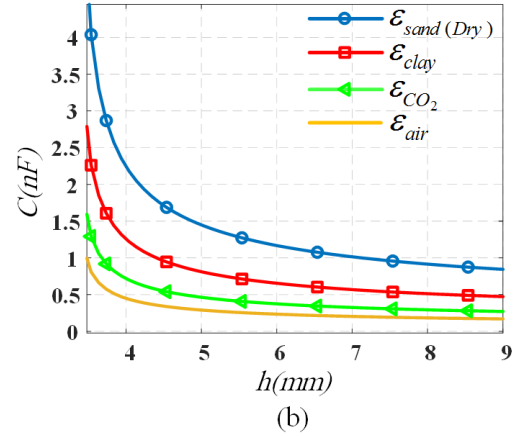
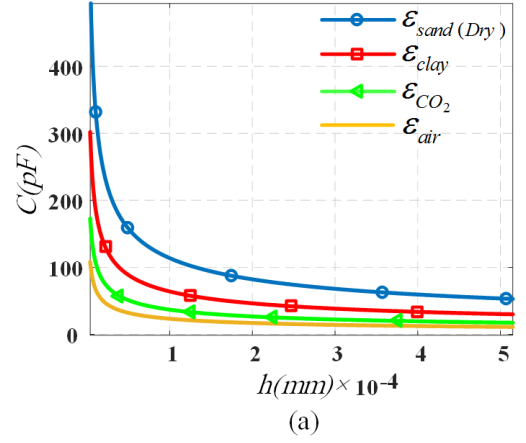


Fig. 4. Impact of dielectric constant and distance to ground on the parasitic capacitance a) in PCBs b) in HV EV cable

Defining two system states as $x_1 = V_{C_{CM}}$ and $x_2 = C_{CM}$, (14) is written in the form of state-space equation as follows:

$$\frac{dx_1}{dt} = \frac{-1}{R_{LISN} x_2} x_1 + \frac{1}{R_{LISN} x_2} u \quad (15)$$

where $u = V_{DS}$ is considered as the system input. In addition, considering that the changes of x_2 in the UKF sampling time interval is very slow one can write:

$$\frac{dx_2}{dt} = 0 \quad (16)$$

A third state variable is defined as $x_3 = \frac{dx_1}{dt}$. Therefore, the third state-space equation can be obtained as follows:

$$\begin{aligned} \frac{dx_3}{dt} &= \frac{d^2 x_1}{dt^2} = \frac{d}{dt} \left(\frac{-1}{R_{LISN} x_2} x_1 + \frac{1}{R_{LISN} x_2} u \right) = \\ &= -\frac{1}{R_{LISN}} \frac{x_2 \frac{dx_1}{dt} - x_1 \frac{dx_2}{dt}}{x_2^2} - \frac{1}{R_{LISN}} \frac{1}{x_2^2} u \xrightarrow{\text{Substituting from (17)}} \\ \frac{dx_3}{dt} &= -\frac{1}{R_{LISN}} \frac{1}{x_2} \left(\frac{-1}{R_{LISN} x_2} x_1 + \frac{1}{R_{LISN} x_2} u \right) - \frac{1}{R_{LISN}} \frac{1}{x_2^2} u = \end{aligned}$$

$$\frac{1}{R_{LISN}^2} \frac{x_1}{x_2^2} - \left(\frac{1}{R_{LISN}^2} + \frac{1}{R_{LISN}} \right) \frac{u}{x_2^2} \quad (17)$$

The CM voltage is also considered as the system output:

$$y = \frac{1}{2} R_{LISN} (2i_{CM}) + v = R_{LISN} C_{CM} \frac{dV_{CM}}{dt} + v = R_{LISN} x_2 x_3 + v \quad (18)$$

Also, to guarantee the observability of the system [38], y is considered as the fourth state variable as follows:

$$x_4 = y \Rightarrow \frac{dx_4}{dt} = R_{LISN} \left(\frac{dx_2}{dt} x_3 + x_2 \frac{dx_3}{dt} \right) = R_{LISN} x_2 \left(\frac{1}{R_{LISN}^2} \frac{x_1}{x_2^2} - \left(\frac{1}{R_{LISN}^2} + \frac{1}{R_{LISN}} \right) \frac{u}{x_2^2} \right) \quad (19)$$

Therefore, the nonlinear state-space equations can be discretized and expressed as follows:

$$\begin{aligned} x_{k+1} &= f(x_k, u_k) + \omega_k \\ y_k &= h(x_k) + v_k \\ \omega_k &\sim (0, Q_k) \\ v_k &\sim (0, R_k) \end{aligned} \quad (20)$$

where $x = [x_1 \ x_2 \ x_3 \ x_4]^T$ is the state vector, ω is the process white noise with zero mean and covariance matrix Q , v is the measurement white noise with zero mean and covariance matrix R , and y is the system output. In the proposed method, the voltage across the line impedance resistance V_{CM} is considered as the output of the system, which can be measured in several ways [34]-[35]. Besides, V_{DS} is considered as the input of the system, which can be measured using some suitable measurement circuitry [37]. In this work, the UKF is adopted for estimation of the parasitic capacitance since it suitably deals with the stochastic nature of the measurement noises and EMI effects [38]-[40]. In the UKF algorithm, first, the state variables and the covariance matrix of the estimation need to be initialized. Since variations of the second state variable are slow, to achieve a suitable response speed, its initial value should be selected as close as possible to its rated value. This requirement can be fulfilled through a pre-calibration stage using some offline tools such as an impedance analyzer. Since four system states are considered in the state-space equation, the covariance matrix of the estimation P has a dimension of 4×4 . Thus, the state vector and P are initialized as follows:

$$\hat{x}_0^+ = [0 \ C_{CM-rated} \ 0 \ 0], \ P_0^+ = I^{4 \times 4} \quad (21)$$

where $C_{CM-rated}$ is the true value of the parasitic capacitance measured with offline tests. Then, the time update from step $(k-1)$ to k is fulfilled as follows:

$$\hat{x}_{k-1}^{(j)} = \hat{x}_{k-1}^+ + \tilde{x}^{(j)} \quad \text{for } j = 1, 2, \dots, 8 \quad (22)$$

where $\tilde{x}^{(j)}$ is the j^{th} sigma point state vector. While different formulations for selecting the sigma points are proposed in the

literature, based on [41], the sigma points are herein chosen according to the following formulas:

$$\begin{aligned} \tilde{x}^{(j)} &= \left(\sqrt{8P_{k-1}^+} \right)_j^T \quad \text{for } j = 1, 2, 3, 4 \\ \tilde{x}^{(j+3)} &= -\left(\sqrt{8P_{k-1}^+} \right)_j^T \quad \text{for } j = 1, 2, 3, 4 \end{aligned} \quad (23)$$

Then, the nonlinear system equation $f(\cdot)$ is used to transform states of (23) into $\hat{x}_k^{(j)}$ vectors as follows:

$$\hat{x}_k^{(j)} = f(\hat{x}_{k-1}^{(j)}, u_k) \quad (24)$$

To obtain the *a priori* state estimate at instant k , the obtained $\hat{x}_k^{(j)}$ are then combined as follows:

$$\hat{x}_k^- = \frac{1}{8} \sum_{j=1}^8 \hat{x}_k^{(j)} \quad (25)$$

Also, the *a priori* estimation of the covariance matrix P is obtained taking into account the process noise as follows:

$$P_k^- = \frac{1}{8} \sum_{j=1}^8 (\hat{x}_k^{(j)} - \hat{x}_k^-) (\hat{x}_k^{(j)} - \hat{x}_k^-)^T + Q_{k-1} \quad (26)$$

The time-update phase can be fulfilled using (25) and (26). For the measurement-update phase, a new set of sigma points can be selected. However, the sigma points (22) can be reused to increase computational efficiency [41]. Therefore, the sigma points of (23) are reused together with the measurement equation $h(\cdot)$ to obtain the $\hat{y}_k^{(j)}$ vectors as follows:

$$\hat{y}_k^{(j)} = h(\hat{x}_k^{(j)}) \quad (27)$$

The $\hat{y}_k^{(j)}$ vectors of (27) are combined to obtain the predicted measurements at instant k as follows:

$$\hat{y}_k = \frac{1}{8} \sum_{j=1}^8 \hat{y}_k^{(j)} \quad (28)$$

The covariance of the predicted measurements is calculated taking the measurement noise into account as follows:

$$P_y = \frac{1}{8} \sum_{j=1}^8 (\hat{y}_k^{(j)} - \hat{y}_k) (\hat{y}_k^{(j)} - \hat{y}_k)^T + R_k \quad (29)$$

Furthermore, the cross-covariance between \hat{y}_k and \hat{x}_k^- is calculated using the following expression:

$$P_{xy} = \frac{1}{8} \sum_{j=1}^8 (\hat{x}_k^{(j)} - \hat{x}_k^-) (\hat{y}_k^{(j)} - \hat{y}_k)^T \quad (30)$$

Finally, the measurement-update phase for the system states and the covariance matrix P is fulfilled using the classical Kalman Filter (KF) equations as follows:

$$\begin{aligned} G_k &= P_{xy} P_y^{-1} \\ \hat{x}_k^+ &= \hat{x}_k^- + G_k (y_k - \hat{y}_k) \\ P_k^+ &= P_k^- - G_k P_y G_k^T \end{aligned} \quad (31)$$

The whole algorithm of the proposed method for estimation of the CM parasitic capacitance is illustrated in Fig. 5.

IV. RESULTS AND DISCUSSIONS

In this section, the simulation and experimental results are provided and discussed to assess the performance of the proposed method in different conditions. For the simulation studies, the system shown in Fig. 2 is simulated using MATLAB/SIMULINK. In the simulation cases, based on a trial and error approach, the covariance matrices of the system and measurement noises are chosen as follows:

$$R = 10^{-2}, Q = 10^{-2} \mathbf{I} \quad (32)$$

Also, all the existing noises in the processed signal such as the measurement noise are included in the calculation to show the performance of the method, realistically. To do so, a random white noise with Signal-to-Noise (SNR) ratio of 30dB is added to the measured values of V_{CM} . In Fig. 6, variations of the CM noise for two different parasitic capacitances are shown. It can be seen that an increase in the value of the parasitic capacitance from 1nF to 10nF substantially increases the noise intensity, which can bring about severe problems in vehicular applications. In Fig. 7, the real and estimated values for typical parasitic capacitances of 0.1nF, 1nF, and 10nF are shown. As seen, the proposed method is able to detect the real values of the parasitic capacitances, efficiently. In addition, it can be seen that the proposed UKF algorithm has an appropriate convergence time. The obtained real-time estimations in the emulated noisy environment show that the proposed method also has good robustness against the measurement noises. In order to confirm the performance of the proposed method in practice, some experiments are also carried out. The experimental test set-up is shown in Fig. 8. In the experiments, the CM equivalent circuit model of Fig. 3(c) is used together with different test capacitors to evaluate the performance of the proposed method. The real values of the test capacitors are measured using an accurate LCR meter. The voltages of V_{DS} and V_{CM} are measured and used in a HIL set-up

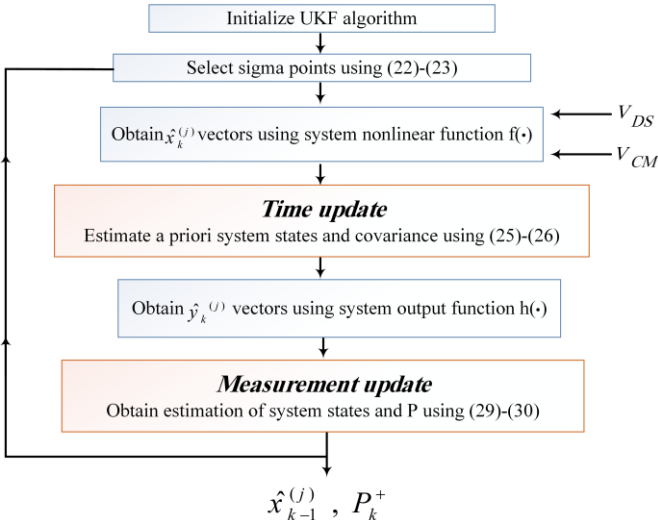


Fig. 5. Algorithm of the proposed method for estimation of the CM parasitic capacitance

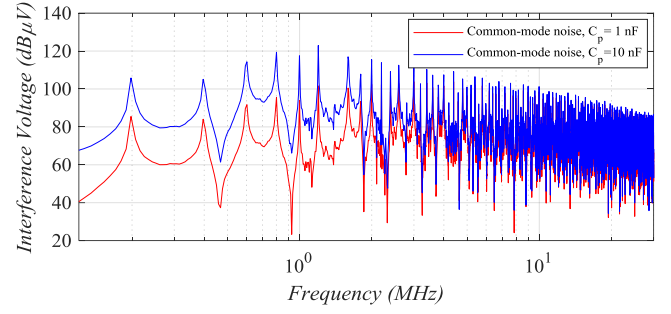


Fig. 6. CM interference voltage for two different values of the parasitic capacitance

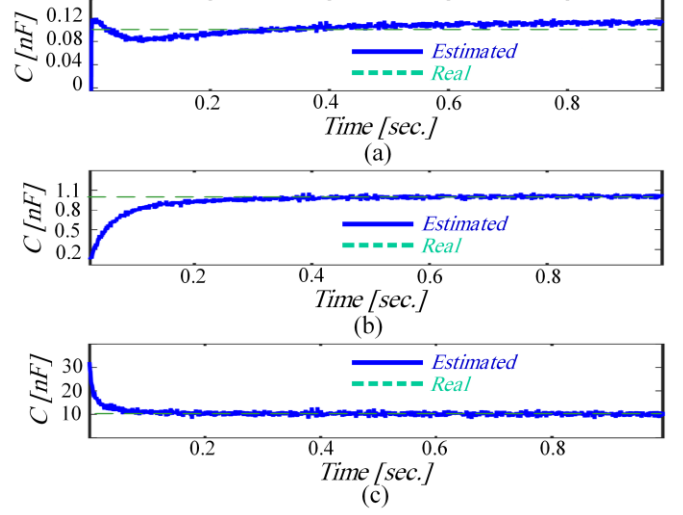


Fig. 7. Real and estimated simulated values of the parasitic capacitance. (a) 0.1nF parasitic capacitance (b) 1nF parasitic capacitance (c) 10nF parasitic capacitance

to estimate the parasitic capacitance. To effectively emulate the CM EMI source, in the implemented equivalent circuit model of Fig. 3(c), V_{DS} is supplied from the studied DC-DC buck converter by a proper interface. In the estimation, the equivalent circuit model of the CM noise shown in Fig. 3(c) is employed. The main problem of the implementation refers to the required high sampling frequency of the processing unit. In fact, for estimation of the very fast dynamics of the nano-farad parasitic capacitances, processors with very high processing frequency are required. Unfortunately, a processor with such processing frequency is not available in our laboratory. Here, a dSPACE1104 data acquisition platform with maximum processing frequency of 250MHz is employed. Therefore, the assessment is carried out for the capacitances in the order of micro-farad as an emulation of the CM parasitic capacitance in the buck converter, which is comprised of the drain-to-ground parasitic capacitance and the HV cables-to-ground parasitic capacitance. In the experiments, the estimation is fulfilled in dSPACE ControlDesk software, in real-time. The estimation results are saved and used in MATLAB for illustration purpose. The UKF algorithm with the same settings as the simulations is reused for the real tests. In Figs. 9(a) to (c), the real-time estimation results for different capacitance values of $47\mu F$, $22\mu F$, and $0.47\mu F$ are shown, respectively. As can be seen, the estimated states suitably converge to their true values after a

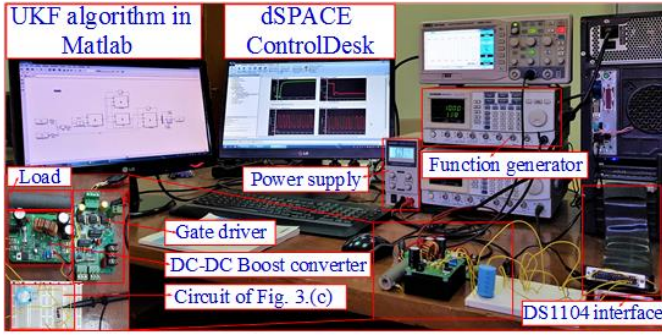


Fig. 8. Experimental test set-up for real-time estimation of the parasitic capacitance

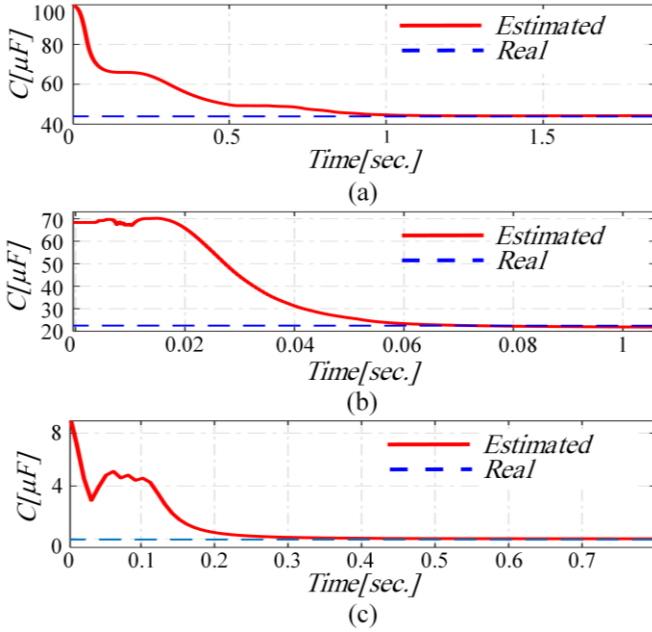


Fig. 9. Experimental real and estimated values of the parasitic capacitance using dSPACE1104 platform. (a) $47 \mu F$ capacitance (b) $22 \mu F$ capacitance (c) $0.47 \mu F$ capacitance

short time. To show the ability of the proposed method in tracking the changes of the parasitic capacitance, some other tests are fulfilled. In these tests, to emulate a change in the value of the parasitic capacitance, a second test capacitor is put in parallel with the base capacitor value after a determined time interval. The relevant estimation results are shown in Fig. 10. In Fig. 10(a), the reference capacitance value changes from $4.7 \mu F$ to $10.7 \mu F$ at $t=4.2$ seconds. It can be seen that not only the initial reference value of the parasitic capacitance is suitably estimated by the designed UKF, but also the proposed method can track the changes in the reference capacitance value. In Fig. 10(b), the estimation results for another scenario in which the reference capacitance value is changed from $4.7 \mu F$ to $5.7 \mu F$ at $t=4$ seconds are shown. The provided results confirm the effectiveness of the designed UKF-based filter for dealing with the varying behaviour of the parasitic capacitance in vehicular applications. Although the proposed method is demonstrated considering a simple DC-DC buck converter, it can be applied to other converter topologies such as the LLC resonant converter [42] with some modifications.

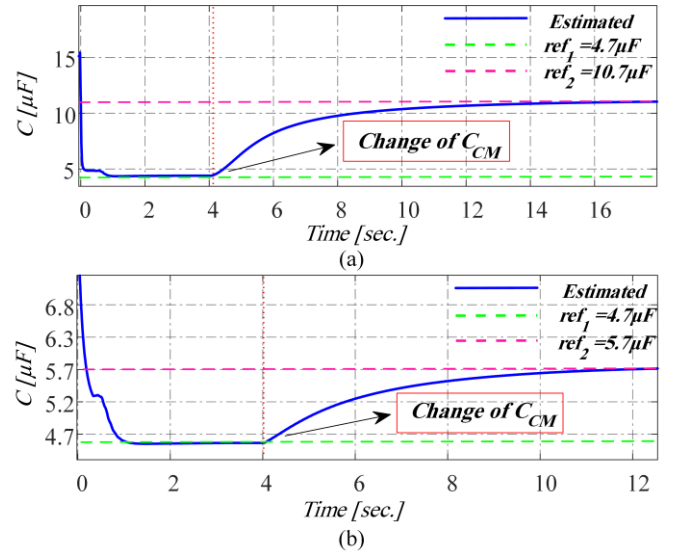


Fig. 10. Experimental estimation results when a change in the value of the capacitance occurs. (a) Estimation results when the reference capacitance changes from $4.7 \mu F$ to $10.7 \mu F$ at $t=4.2$ sec. (b) Estimation results when the reference capacitance changes from $4.7 \mu F$ to $5.7 \mu F$ at $t=4$ sec.

V. COMPUTATIONAL PERFORMANCE OF THE PROPOSED APPROACH

In this section, the real-time performance of the proposed UKF-based approach in both simulation and experiment are discussed. The simulations of the proposed method are carried out in MATLAB/SIMULINK on a computer with Intel Core i7-5960X 3.00 GHz CPU and 32 GB of RAM. The model execution performance is evaluated using the SIMULINK Desktop Real-Time™ Blockset. The real-time performance results are shown in Fig. 11. As seen in Fig. 11, the execution time changes from one sample to another because of the random function of the CPU cache. A good estimation of the computational time, however, can be obtained by averaging the computation time over a large number of samples, which led to an average computational time of about $5.1588506e-07$. Therefore, when the sampling time of the UKF is set to $10 \mu s$, almost 5% of the CPU resource will be occupied by the algorithm. The real-time computational burden of the proposed algorithm in experimental cases are also calculated. Specifically, the required computation time and percentage of the occupied CPU resource for real-time estimation of the parasitic capacitances (described in Section IV) using the dSPACE1104 development platform were determined. The dSPACE1104 card has a sampling frequency of 250 MHz with an overall 32 MB of SDRAM. To fulfill the experimental real-time tests, the UKF algorithm is implemented in MATLAB/SIMULINK environment with a sampling frequency of $10 \mu s$. Then, the required description file (.sdf file) for using in ControlDesk software is generated using MATLAB Coder option. The calculation of the computational time is carried out using dSPACE Real-Time Interface (RTI) via *atomic subsystems*. The calculated average execution time of the proposed algorithm is about $3.2935e-06$ seconds, which means that about 32% of the CPU resource of the dSPACE1104 will be occupied by the implemented UKF

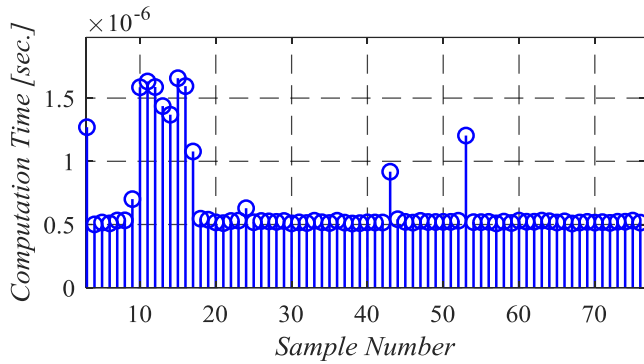


Fig. 11. Computational time of the UKF algorithm with MATLAB the simulations on a system with 3.00 GHz CPU and 32 GB of RAM

codes. The foregoing real-time tests show the feasibility of the proposed approach for online estimation of the parasitic capacitances from a few μF to hundreds of pF.

VI. IMPLEMENTATION CHALLENGES AND POTENTIAL SOLUTIONS

The real-time implementation of the proposed method for online estimation of the parasitic capacitance requires state-of-the-art processing and measuring technologies. Unfortunately, the authors did not access to all of these requirements for performing tests in the pF range. Anyhow, the main challenges and the corresponding solutions are discussed in detail in this section. Technically, for implementation of the proposed method, one microprocessor and two voltage sensors for measuring the CM voltage and drain-source voltage of the MOSFET are required. As the parasitic capacitance of the CM noise can be as small as the pico-farad level, a microprocessor with high enough processing frequency in the range of GHz is needed. There are some analog voltage measurement circuitry for measuring the drain-source voltage of the semiconductor switches, which can also be utilized in this work. Using such a technique for the measurement, an Analog-to-Digital Converter (ADC) and a processing unit with high enough frequency are needed, which are generally integrated into the microprocessors. Some of the commercial Digital Signal Processors (DSPs) and/or Field Programmable Gate Arrays (FPGAs) can handle this implementation.

In this work, for simplicity and ease of illustration, the CM voltage is measured considering the LISN structure. However, for real implementation, other approaches for measuring the CM voltage without using the LISN can also be used [43]-[44].

It must be emphasized that real-time estimation of the parasitic capacitance of the CM noise is a novel concept, which is proposed in this work for the first time. The application of this concept is of critical importance for MEAs, EVs, and satellites in which variations of the environmental and operating conditions result in unforeseeable fluctuations in the EMI level. In such applications, reliability is a critical index, which justifies increasing the investment cost to some extent for adoption of the proposed approach. The processing capability of the microprocessors has shown a significant increasing trend in recent years. Hence, it is expected that more powerful and less expensive microprocessors will be available soon, which eases the adoption of the presented technique.

VII. CONCLUSION

In this paper, the real-time estimation of parasitic capacitance in a typical DC-DC buck converter is investigated. Using the equivalent circuit of the CM noise and a UKF as a state estimator, the effective parasitic capacitance is estimated in real-time. The presented results show that the designed UKF algorithm can estimate the value of the parasitic capacitance in real-time. It is validated that the variation of the parasitic capacitance is remarkable in vehicular applications such as MEAs and EVs, which should be tackled using an efficient filter for all conditions. Therefore, real-time estimation is necessary for the adjustment of such a filter. Implementation of such a technique has some challenges in practice, which are discussed and some solutions for them are also suggested.

REFERENCES

- [1] C. R. Paul, Introduction to Electromagnetic Compatibility, 2nd ed. New York, NY, USA: Wiley, 2006.
- [2] R. Zhu, N. Lin, V. Dinavahi, and G. Liang, "An Accurate and Fast Method for Conducted EMI Modeling and Simulation of MMC-Based HVDC Converter Station," *IEEE Trans. Power Electron.*, vol. 35, no. 5, pp. 4689-4702, May 2020.
- [3] J. Wang, X. Liu, Y. Xun, and S. Yu, "Common Mode Noise Reduction of Three-Level Active Neutral Point Clamped Inverters With Uncertain Parasitic Capacitance of Photovoltaic Panels," *IEEE Trans. Power Electron.*, vol. 35, no. 7, pp. 6974-6988, July 2020.
- [4] E. Rondon-Pinilla, F. Morel, C. Vollaie, and J.L. Schanen, "Modeling of a Buck Converter With a SiC JFET to Predict EMC Conducted Emissions," *IEEE Trans. Power Electron.*, vol. 29, no. 5, pp. 2246-2260, May 2014.
- [5] P. Kong, Y. Jiang and F. C. Lee, "Common Mode EMI Noise Characteristics of Low-Power AC-DC Converters," *IEEE Trans. Power Electron.*, vol. 27, no. 2, pp. 731-738, Feb. 2012.
- [6] A. S. de Beer and K. Faul, "Factors Influencing Common Mode EMI Generation in Boost Converters," *IEEE Global Electromagn. Compat. Conf.*, 2018, pp. 1-5.
- [7] S. Wang, P. Kong, and F. C. Lee, "Common mode noise reduction for boost converters using general balance technique," *IEEE Trans. Power Electron.*, vol. 22, no. 4, pp. 1410-1416, Jul. 2007.
- [8] P. Kong, S. Wang, F. C. Lee, and C. Wang, "Common mode EMI study and reduction technique for the interleaved multi-channel PFC converter," *IEEE Trans. Power Electron.*, vol. 23, no. 5, pp. 2576-2584, Sep. 2008.
- [9] H. L. Chen, C. Chen and Y. C. Ren, "Modeling and characterization of incomplete shielding effect of GND on common-mode EMI of a power converter," *IEEE Trans. Electromagn. Compat.*, vol. 53, no. 3, pp. 676-683, Aug. 2011.
- [10] M. Moon et al., "Modeling and analysis of return paths of common mode EMI noise currents from motor drive system in hybrid electric vehicle," *Asia-Pac Symp. on Electromagn. Compat.*, Taipei, 2015, pp. 82-85.
- [11] J. Luszcz, "Motor cable effect on the converter fed AC motor common mode current," *7th Int. Conf-Workshop Compat. and Power Electron. (CPE), Tallinn*, 2011, pp. 445-450.
- [12] H. de Paula, M. V. C. Lisboa, J. F. R. Guilherme, W. P. de Almeida and M. L. R. Chaves, "Differential overvoltages and common-mode currents in PWM motor drives: The influence of the cable arrangement on their characteristics," *2009 35th Annual Conf. of IEEE Ind. Electron.*, Porto, 2009, pp. 1103-1109.
- [13] F. Costa, C. Vollaie and R. Meuret, "Modeling of conducted common mode perturbations in variable-speed drive systems," *IEEE Trans. Electromagn. Compat.*, vol. 47, no. 4, pp. 1012-1021, Nov. 2005.
- [14] L. Xie, X. Ruan, H. Zhu and Y. Lo, "Common-Mode Voltage Cancellation for Reducing the Common-Mode Noise in DC-DC Converters," *IEEE Trans. Ind. Electron.*
- [15] C. Wu et al., "Analysis and Modeling of Conducted EMI from an AC-DC Power Supply in LED TV up to 1 MHz," *IEEE Trans. Electromagn. Compat.*, vol. 61, no. 6, pp. 2050-2059, Dec. 2019.
- [16] L. Yang, H. Zhao, S. Wang and Y. Zhi, "Common-Mode EMI Noise Analysis and Reduction for AC-DC-AC Systems With Paralleled Power

Modules,” *IEEE Trans. Power Electron.*, vol. 35, no. 7, pp. 6989-7000, July 2020.

[17] Y. Xiang, X. Pei, W. Zhou, Y. Kang and H. Wang, “A Fast and Precise Method for Modeling EMI Source in Two-Level Three-Phase Converter,” *IEEE Trans. Power Electron.*, vol. 34, no. 11, pp. 10650-10664, Nov. 2019.

[18] X. Gong, I. Josifović and J. A. Ferreira, “Modeling and Reduction of Conducted EMI of Inverters With SiC JFETs on Insulated Metal Substrate,” *IEEE Trans. Power Electron.*, vol. 28, no. 7, pp. 3138-3146, July 2013.

[19] S. Karimi, E. Farjah and T. Ghanbari, “Common and Differential Modes of Conducted Electromagnetic Interference in Electric Vehicle equipped with Supercapacitor,” *10th Int. Power Electron., Drive Systems and Technol. Conf. (PEDSTC)*, Shiraz, Iran, 2019, pp. 653-658.

[20] H. Qin, C. Ma, Z. Zhu, and Y. Yan, “Influence of Parasitic Parameters on Switching Characteristics and Layout Design Considerations of SiC MOSFETs,” *J. Power Electron.*, vol. 18, no. 4, pp. 1255-1267, 2018.

[21] L. Wang, J. Yang, H. Ma, Z. Wang, K. O. Olanrewaju, K. D. E. Kerrouche, “Analysis and Suppression of Unwanted Turn-On and Parasitic Oscillation in SiC JFET-Based Bi-Directional Switches,” *Electronics*, vol. 7, no. 8, pp. 126, Jul. 2018.

[22] X. Gong, I. Josifović and J. A. Ferreira, “Modeling and Reduction of Conducted EMI of Inverters With SiC JFETs on Insulated Metal Substrate,” *IEEE Trans. Power Electron.*, vol. 28, no. 7, pp. 3138-3146, July 2013.

[23] Huibin Zhu, A. R. Hefner and J. - Lai, “Characterization of power electronics system interconnect parasitics using time domain reflectometry,” *IEEE Trans. Power Electron.*, vol. 14, no. 4, pp. 622-628, July 1999.

[24] M. Trivedi and K. Shenai, “Parasitic extraction methodology for insulated gate bipolar transistors,” *IEEE Trans. Power Electron.*, vol. 15, no. 4, pp. 799-804, July 2000.

[25] N. Hadjigeorgiou, and P. P. Sotiriadis, “Parasitic Capacitances, Inductive Coupling and High-Frequency Behavior of AMR Sensors,” *IEEE Sensors J.*, vol. 20, no. 5, March 1, 2020

[26] H. Chen, C. Chen and Y. Ren, “Modeling and Characterization of Incomplete Shielding Effect of GND on Common-Mode EMI of a Power Converter,” *IEEE Trans. Electromagn. Compat.*, vol. 53, no. 3, pp. 676-683, Aug. 2011.

[27] H. M. Al-Rizzo and H. T. Al-Hafid, “Measurements of the complex dielectric constant of sand and dust particles at 11 GHz,” *IEEE Trans. Instrum. Meas.*, vol. 37, no. 1, pp. 110-113, March 1988.

[28] Seyfried, M.S., and L.E. Grant. “Temperature effects on soil dielectric properties measured at 50 MHz,” *Vadose Zone J.* 6(4):759-765. 2007.

[29] Bhuyan, B. Tudu, R. Bandopadhyay, A. Ghosh, and S. Kumar, “Extended Kalman Filtering for Estimation of Parasitic Artifacts in Three Electrode Electrochemical Sensors,” *IEEE Sensors Lett.*, vol. 3, no. 10, pp. 1-4, 2019.

[30] S. Wang and F. C. Lee, “Common-Mode Noise Reduction for Power Factor Correction Circuit With Parasitic Capacitance Cancellation,” *IEEE Trans. Electromagn. Compat.*, vol. 49, no. 3, pp. 537-542, Aug. 2007.

[31] Q. Ji, X. Ruan and Z. Ye, “The Worst Conducted EMI Spectrum of Critical Conduction Mode Boost PFC Converter,” *IEEE Trans. Power Electron.*, vol. 30, no. 3, pp. 1230-1241, March 2015.

[32] E. Bogatin, “Design rules for microstrip capacitance,” *IEEE Trans. Compon. Hybrids Manuf. Technol.*, vol. 11, no. 3, pp. 253-259, Sept. 1988.

[33] M. S. Zamik, D. Belavic, “An experimental and numerical study of the humidity effect on the stability of a capacitive ceramic pressure sensor,” *Radioengineering*, vol. 21, no. 1, pp. 201, Apr. 2012.

[34] C. Paul, *Analysis of Multiconductor Transmission Lines*, New York:Wiley, 1994.

[35] K. Li, K. See and R. M. Sooriya Bandara, “Impact Analysis of Conducted Emission Measurement Without LISN,” *IEEE Trans. Electromagn. Compat.*, vol. 58, no. 3, pp. 776-783, June 2016.

[36] M. C. Di Piazza, G. Tine and G. Vitale, “An Improved Active Common-Mode Voltage Compensation Device for Induction Motor Drives,” *IEEE Trans. Ind. Electron.*, vol. 55, no. 4, pp. 1823-1834, April 2008.

[37] P. Asimakopoulos, K. D. Papastergiou, T. Thiringer, A. M. Bongiorno, G. L. Godec, “On V ce method: in-situ temperature estimation and aging detection of high-current IGBT modules used in magnet power supplies for particle accelerators,” *IEEE Trans. Ind. Electron.*, vol. 66, no. 1, pp. 551-560, Jan. 2019.

[38] F. Naseri, E. Farjah, T. Ghanbari, Z. Kazemi, E. Schaltz and J. L. Schanen, “Online parameter estimation for supercapacitor state-of-energy and state-of-health determination in vehicular applications,” *IEEE Trans. Ind. Electron.*, vol. 67, no. 9, 2020.

[39] F. Naseri, Z. Kazemi, M. M. Arefi, and E. Farjah, “Fast discrimination of transformer magnetizing current from internal faults: An extended Kalman filter-based approach,” *IEEE Trans. Power Del.*, vol. 33, no. 1, pp. 110-118, 2018.

[40] F. Naseri, Z. Kazemi, E. Farjah, and T. Ghanbari, “Fast Detection and Compensation of Current Transformer Saturation Using Extended Kalman Filter,” *IEEE Trans. Power Del.*, vol. 34, no. 3, pp.1087-1097, 2019.

[41] D. Simon, “*Optimal state estimation: Kalman, H infinity, and nonlinear approaches*,” John Wiley & Sons. 2006.

[42] D. Fu, S. Wang, P. Kong, F. C. Lee and D. Huang, “Novel Techniques to Suppress the Common-Mode EMI Noise Caused by Transformer Parasitic Capacitances in DC-DC Converters,” *IEEE Trans. Ind. Electron.*, vol. 60, no. 11, pp. 4968-4977, Nov. 2013.

[43] L. Ran, J. C. Clare, K. J. Bradley and C. Christopoulos, “Measurement of conducted electromagnetic emissions in PWM motor drive systems without the need for an LISN,” *IEEE Trans. Electromagn. Compat.*, vol. 41, no. 1, pp. 50-55, Feb. 1999.

[44] K. Li, K. See and R. M. Sooriya Bandara, “Impact Analysis of Conducted Emission Measurement Without LISN,” *IEEE Trans. Electromagn. Compat.*, vol. 58, no. 3, pp. 776-783, June 2016.



Sepehr Karimi was born on March 21st, 1994 in Darab city, Shiraz province, Iran. He received the B.Sc. degree in electrical engineering from Arak University of Technology, Arak, Iran, in 2016. He is now pursuing M.Sc. degree in electrical power engineering in Shiraz University. His research interests include power electronics, electromagnetic compatibility analysis, electric vehicles, and state estimation.



Ebrahim Farjah received the B.Sc. degree in electrical and electronics engineering from Shiraz University, Iran, in 1987, the M.Sc. degree in electrical power engineering from Sharif University of Technology, Tehran, Iran, in 1989, and the Ph.D. degree in electrical engineering from Grenoble Institute of Technology, Grenoble, France. He is currently a Professor in the Department of Electrical and Computer Engineering of Shiraz University. His research interests include power electronics, renewable energy, micro-grids, and power quality.



Teymoor Ghanbari received the B.Sc. degree in Electrical Power Engineering from S.R. University, Tehran, Iran, the M.Sc. degree from Shahrood University of Technology, Shahrood, Iran, and the Ph.D. degree in the same field from Shiraz University, Shiraz, Iran. He is currently an Associate Professor in the School of Advanced Technologies of Shiraz University. His research interests include distributed generation, power electronics, and electrical machines.



Farshid Naseri received the B.Sc. degree in electrical engineering from Shiraz University of Technology, Shiraz, Iran, in 2013, and the M.Sc. degree in electrical power engineering from Shiraz University, Shiraz, Iran, in 2015. He is now pursuing Ph.D. degree in electrical power engineering in Shiraz University. Between July to October 2019, Farshid worked as a guest researcher at the Department of Energy Technology, Aalborg University, Aalborg, Denmark where he has joined the Electro-Mobility and Industrial Drives research program. He has published over 23 scientific articles in his field and has been serving as a reviewer in many top IEEE journals. His

research interests include power electronics, electric vehicles, and state estimation.



Jean-Luc Schanen (M'99–SM'04) received the Electrical Engineering Diploma and the Ph.D. degrees from the Grenoble Institute of Technology, Grenoble, France, in 1990 and 1994, respectively. He is Professor with at Univ Grenoble Alpes since 2003 and is leading the power electronics research group of G2ELab. His research activities are focused on the technological design of Power Electronics systems, including EMC aspects. His group

develops models and tools for Power Converters optimization. He is past chair of the IEEE-IAS Power Electronics Devices and Components Committee, acts as Associate Editor for many IEEE Journals and is member of several conferences steering committees.